Icarus 410 (2024) 115918

Contents lists available at ScienceDirect

Icarus

journal homepage: www.elsevier.com/locate/icarus

Paleoenvironment implications of layered ejecta craters in the Chryse Planitia, Mars

Sheng Gou [a,b,c], Zongyu Yue [b,c,d], Kaichang Di [b,d,*], Roberto Bugiolacchi [a,e], Shengli Niu [a,f], Zhanchuan Cai [a], Bin Liu [b], Shuanggen Jin [g,h]

[a] State Key Laboratory of Lunar and Planetary Sciences, Macau University of Science and Technology, Macau 999078, China
[b] State Key Laboratory of Remote Sensing Science, Aerospace Information Research Institute, Chinese Academy of Sciences, Beijing 100101, China
[c] Key Laboratory of Earth and Planetary Physics, Institute of Geology and Geophysics, Chinese Academy of Sciences, Beijing 100029, China
[d] Center for Excellence in Comparative Planetology, Chinese Academy of Sciences, Hefei 230026, China
[e] Earth Sciences, University College London, London WC1E 6BT, UK
[f] State Key Laboratory of Space Weather, National Space Science Center, Chinese Academy of Sciences, Beijing 100190, China
[g] Shanghai Astronomical Observatory, Chinese Academy of Sciences, Shanghai 200030, China
[h] School of Surveying and Land Information Engineering, Henan Polytechnic University, Jiaozuo 454003, China

ARTICLE INFO

Keywords:
Layered ejecta craters (LECs)
Chryse Planitia
Fluvial activities
Temporal-spatial evolution
Volatile-rich layer

ABSTRACT

The formation of martian layered ejecta craters (LECs), which have one or multiple distinctive fluidized layered ejecta deposits, is generally hypothesized to be directly related to subsurface volatiles. Using a high-resolution (5 m/pixel) context camera (CTX) mosaic as a base map, 525 LECs (including 157 newly identified) were catalogued in the Chryse Planitia and divided into three types according to the number of layered ejecta, i.e., single layer ejecta (SLE), double layer ejecta (DLE), and multiple layer ejecta (MLE). It is found that the minimum crater diameter (here called the onset diameter) decreases with increasing latitude, and could be as small as 1 km. The average ejecta mobility (EM) values usually increase from the low to the high latitude interval for each LEC type and gradually increase with the number of layered ejecta within each latitude interval. The lobateness values of the SLE craters have a decreasing trend with increasing latitude, however, such a trend is not obvious for the DLE and MLE craters. The absolute model ages (AMAs) of 135 LECs were determined from the crater size-frequency distribution (CSFD) method to constrain the timing of the fluvial activities of the circum-Chryse outflow channels and to investigate the local temporal-spatial evolution of the subsurface volatile-rich layer. The superposition relationship between the LECs and circum-Chryse channels suggests fluvial activity might have extended into the early Amazonian. Floods that carved the Ares, Tiu, and Simud Valles likely ended before ~μ2.7 Ga, while those relating to theVedra, Manmee, and Maja Valles ceased between ~μ2.2 Ga and ~ μ1.9 Ga. The fluvial resurfacing activities in the Kasei Valles likely did not last past ~μ2.8 Ga. The dating results and excavation depths of LECs (diam. < 6 km) suggest that the minimal roof depth of the volatile-rich layer has remained relatively stable at least around 560– 590 m since the early Amazonian, and regional differences indicate that it could be as shallow as ~440 m at high latitudes and ~540 m at low latitudes.

1. Introduction

Impact cratering, one of the prominent geomorphological modifiers of the martian surface, potentially allows inferences about the subsurface composition and properties. Layered ejecta craters (LECs), which are characterized by one or multiple distinctive fluidized layered ejecta deposits (Fig. 1), were first identified on the martian surface from images acquired by the Mariner 9 mission (McCauley, 1973). The layered ejecta morphology differs notably from the radial ejecta patterns that are typical of craters on other planetary bodies, e.g., the Moon and Mercury. Mechanisms of formation other than simple ballistic emplacement have been proposed, e.g., atmospheric drag/entrainment model (Schultz and Gault, 1979; Barnouin-Jha and Schultz, 1998), subsurface volatile fluidization model (Carr et al., 1977; Mouginis-Mark,

* Corresponding author at: State Key Laboratory of Remote Sensing Science, Aerospace Information Research Institute, Chinese Academy of Sciences, Beijing 100101, China.
E-mail address: dikc@radi.ac.cn (K. Di).

https://doi.org/10.1016/j.icarus.2023.115918
Received 4 August 2023; Received in revised form 30 November 2023; Accepted 5 December 2023
Available online 10 December 2023

1987), and a combination of both the atmosphere drag and volatile fluidization models (Barlow, 2005; Komatsu et al., 2007). For instance, layered ejecta deposits on Venus are hypothesized to have been emplaced through interactions with the planet's thick atmosphere under anhydrous conditions (Schultz, 1992; Barlow and Robbins, 2015). However, LECs have also been found on airless bodies, e.g., Europa (Moore et al., 2001), Ganymede (Boyce et al., 2010), and even Ceres (Hughson et al., 2019). Consequently, it is generally agreed that the formation of these craters is mostly due to the presence of subsurface volatiles, in particular, ice and/or water, which fluidize the ejecta blankets upon impact (Barlow, 2005; Boyce et al., 2010; Weiss and Head, 2017).

Previous studies have revealed that LECs are ubiquitous on the martian surface, although with the minimum crater diameter (here called the onset diameter) showing a latitude dependence (Mouginis-Mark, 1979; Kuzmin et al., 1988; Costard, 1989; Barlow and Bradley, 1990; Barlow and Perez, 2003; Barlow, 2006; Robbins and Hynek, 2012b; Jones and Osinski, 2015; Li et al., 2015; Lagain et al., 2021b). For instance, the onset diameters are typically 4 to 7 km in the equatorial regions and are 1 to 2 km at high latitudes (50° latitudes) (Squyres et al., 1992), suggesting a volatile-rich layer at depths of about 300– 400 m near the equator and about 50– 100 m at 50° latitudes (Kuzmin et al., 1988). Subsequent studies have revealed that the equatorial onset diameter varies regionally (Barlow et al., 2001) and can be as small as 1 km in Hesperian Valles Marineris Plateaus (Reiss et al., 2005).

Using the Thermal Emission Imaging System (THEMIS) daytime infrared mosaic (100 m/pixel) as a base map, Robbins and Hynek (2012b), Barlow (2015), and Li et al. (2015) discovered a large number of LECs on the martian surface, suggestive of the presence of one or multiple volatile-rich layer(s) at the time of impact. However, due to the limitation in image resolution, only LECs with a diameter >5 km (Barlow, 2015), 3 km (Robbins and Hynek, 2012b), and 1.5 km (Li et al., 2015) were included in their respective research. With the release of the global high–resolution (5 m/pixel) context camera (CTX) mosaic (Dickson et al., 2018), it is now possible to re-investigate and catalogue LECs of much smaller sizes down to about one kilometer in diameter. In addition, Squyres et al. (1992) suggested that the LECs may have formed over a significant time interval and that the onset diameter reflects the volatile depth at a given time. Subsequent studies have supported this hypothesis (Barlow, 2004; Kadish and Head, 2014; Jones, 2015), although without deriving the temporal-spatial geological evolution of the subsurface volatile-rich layer.

As the LECs play an important role in interpreting the subsurface volatiles, this study plans to take full advantage of the CTX mosaic to catalogue the LECs in a region where many have already been identified (Robbins and Hynek, 2012a; Li et al., 2015; Lagain et al., 2021b), i.e., Chryse Planitia and tries to investigate their paleoenvironment implications, e.g., the timing of the fluvial activities of the circum-Chryse outflow channels and the temporal-spatial evolution of the subsurface volatile-rich layer.

2. Study area

The Chryse Planitia, located within the northern lowlands near the Mars dichotomy (Fig. 2a-b), represents an ancient, giant impact basin that was subsequently flooded and severely eroded (Schultz et al., 1982; Carr and Head, 2010; Pan et al., 2019). The formation of LECs is usually hypothesized to be directly related to the presence of subsurface volatiles, which might be historically recharged by the outflow channels surrounding Chryse Planitia (Carr and Head, 2010). Consequently, the Chryse Planitia represents an ideal survey place for a detailed mapping of LECs.

Chryse Planitia is a smooth, quasi-circular plain ~1500 km in diameter with an average altitude of −3.7 km (Fig. 2c-d). Due to the general topography and setting being broadly similar to that of the Isidis basin, a giant impact origin for the Chryse Planitia was first hypothesized by Schultz et al. (1982) and subsequently validated by Pan et al. (2019). The Chryse Planitia has been associated with an ancient large body of water (Parker et al., 1993; Moore et al., 1995), from which many giant Hesperian circum-Chryse outflow channels debouched and fed into the northern lowlands, e.g., Kasei Valles, Vedra Valles, Maumee Valles, Maja Valles, Tiu Valles, Simud Valles, and Ares Vallis (Fig. 2a) carving out huge channels and teardrop-shaped islands. To search for signs of life and past fluvial processes, the Viking 1 (Mutch et al., 1976) and the Mars Pathfinder (Golombek et al., 1997) missions targeted the Chryse Planitia and conducted in situ measurements and experiments (Fig. 2a). However, the surface of the Viking 1 landing area was found to be a boulder-strewn desert with a distinctively reddish hue with both impact and aeolian processes being evident (Mutch et al., 1976). In contrast, rounded pebbles and cobbles in the Mars Pathfinder landing area are suggestive of lasting fluvial processes, implying liquid water in equilibrium with the atmosphere and thus a warmer and wetter past was suggested (Golombek et al., 1997).

The maximum elevation difference between the Chryse Planitia and surrounding terra is about 8000 m (Fig. 2a) and several geological units have been proposed to characterize its surface (Fig. 2b). However, the study area (outlined by the black dashed circle in Fig. 2a) is located within the relatively flat bottom of the Chryse basin, with height differences in most locations being <700 m (Fig. 2c-d). It is largely dominated by the Hesperian transition outflow (Hto) unit and late Hesperian lowland (lHl) unit (Fig. 2b). Therefore, the study area is considered morphologically uniform, and its geological diversity and

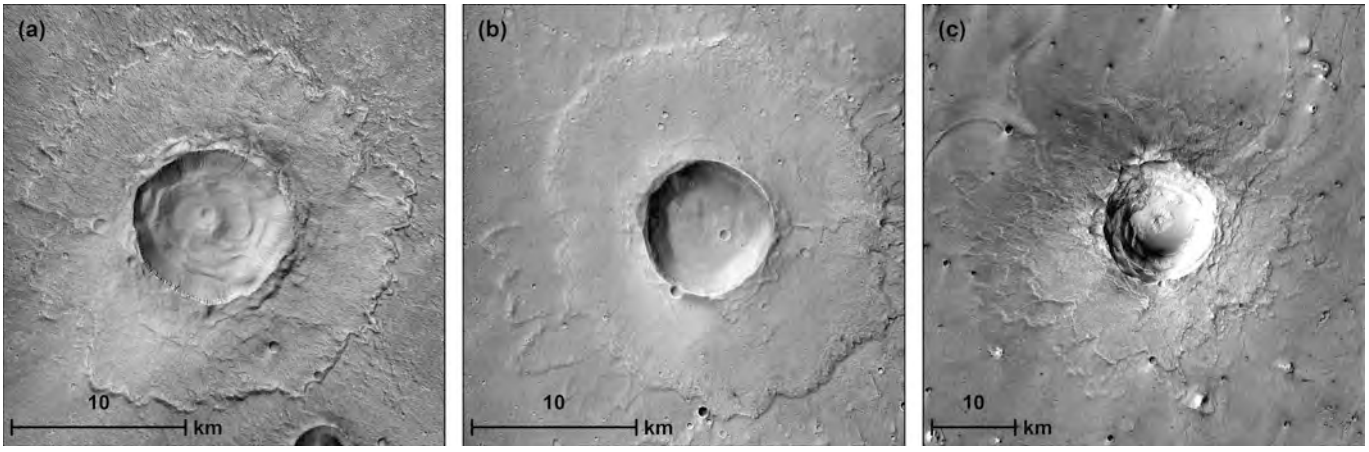

Fig. 1. Examples of different types of LECs. (a) single layer ejecta crater (41.63°W, 27.05°N, D = 9.3 km); (b) double layer ejecta crater (51.24°W, 23°N, D = 8.5 km); (c) multiple layer ejecta crater (34.17°W, 29.57°N, D = 13.8 km).

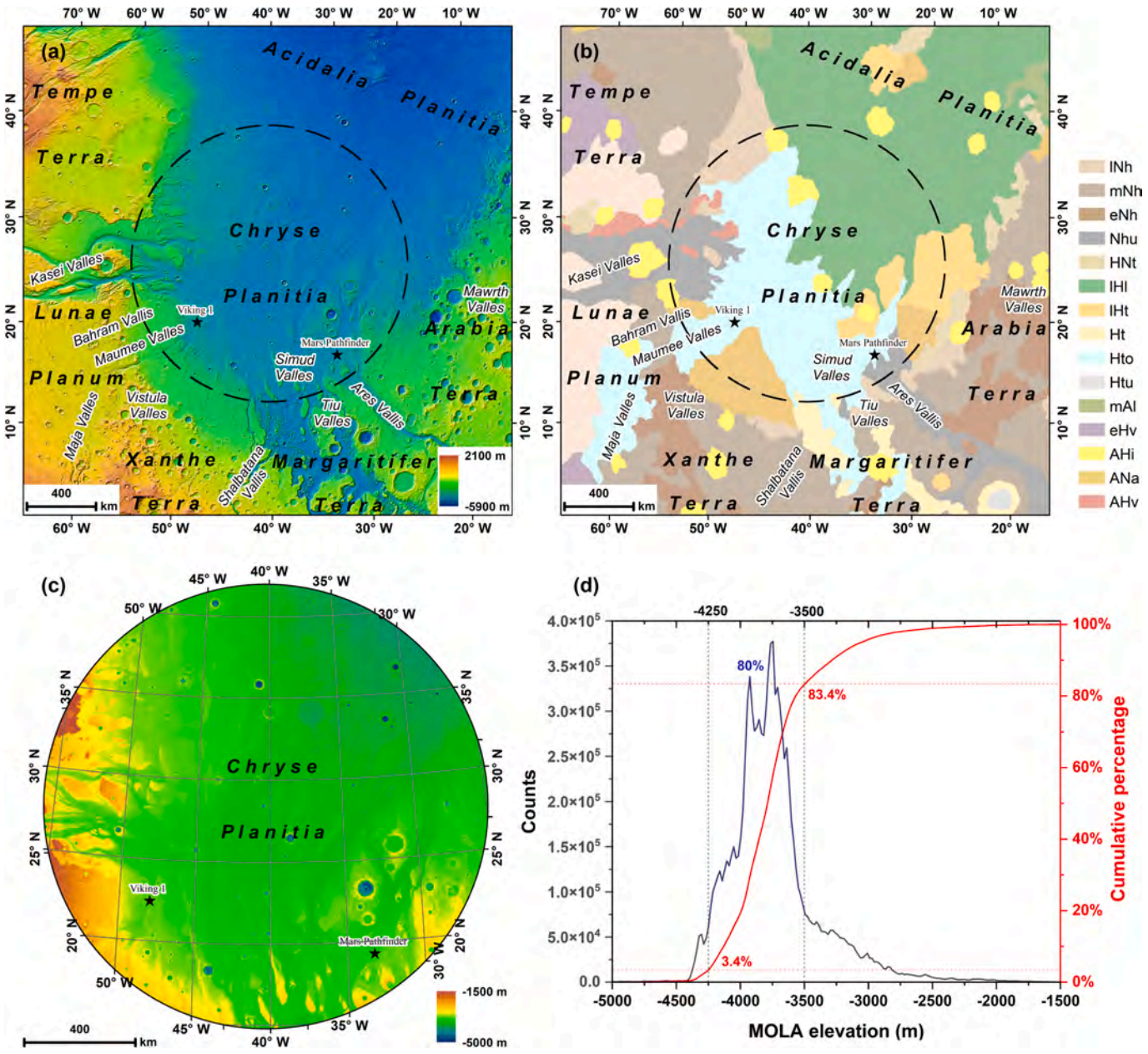

Fig. 2. (a)Mars Orbiter Laser Altimeter (MOLA) (Smith et al., 2001) topography context of the Chryse Planitia and surrounding terra. (b) Geology map of the Chryse Planitia and surrounding terra (Tanaka et al., 2014). (c) MOLA elevation of the study area. (d) Histogram of MOLA elevation of the study area. (a)-(c) are shown in orthographic projection with center at 40°W, 28°N. The dashed circle marks the approximate boundary of the Chryse Planitia, i.e., the study area.

elevation should have only a marginal impact on the objectives of this study.

3. Data and methods

3.1. CTX and THEMIS mosaic

The context camera (CTX) onboard the Mars Reconnaissance Orbiter (MRO) spacecraft is a push-broom imager, which acquires 30-km-wide, ≥40-km-long, 5–6.5 m/pixel views of the martian surface from a nominal 255–320 km altitude orbit (Malin et al., 2007). The CTX has mapped about 99% of the martian surface after taking >125,000 images since the MRO spacecraft began observing Mars from orbit in 2006 (Robbins et al., 2023). A high resolution (5 m/pixel) CTX mosaic (beta01 version) (Dickson et al., 2018) that covers the entire Chryse Planitia is used as a base map in this study for the identification of LECs and crater counting on their ejecta blankets.

In some local areas of the CTX mosaic, the low contrast leads to the inability to accurately identify the boundary of the layered ejecta. Consequently, the Thermal Emission Imaging System (THEMIS)-daytime infrared (IR) 100 m/pixel mosaic (Edwards et al., 2011) is also used as an ancillary in this study.

3.2. Identification and classification of LECs

LECs in the Chryse Planitia are mapped by their distinctive layered ejecta morphologies and compared with the Mars crater databases created by Robbins and Hynek (2012a), Li et al. (2015), and Lagain et al. (2021b) to show the newly reported LECs in this study. The identified LECs are subdivided into three types according to the number of layered ejecta, i.e., single layer ejecta (SLE), double layer ejecta (DLE), and multiple layer ejecta (MLE) (Barlow et al., 2000), with attributes of the

ejecta patterns being attached, i.e., rampart (R), pancake (P), sinuous (S), circular (C), radial (Rd), large aspect ratio (LAR). For example, a single layer ejecta crater with sinuous rampart ejecta that has a radial pattern superposed on it is recorded as "SLERS/Rd" in the catalogue.

Based on the work done by Robbins and Hynek (2012a), the LECs were also categorized according to crater shape, i.e., simple (Smp) bowl-shaped crater or complex (Cpx) crater, with additional morphologic attributes recommended by Barlow and Bradley (1990) being also recorded, i.e., flat floor (FF), central peak (CPk), central pit (CPt), summit pit (SuPt), unclassifiable/chaotic (Unc). For example, a complex crater with a central peak is recorded as "CpxCPk" in the catalogue.

3.3. Determination of the formation time of LECs

3.3.1. Absolute model age determination

To constrain the formation time of the LECs, the absolute model ages (AMAs) are determined by applying the crater counting technique to a geological unit to fit the observed crater size-frequency distribution (CSFD) with an isochron (derived from a production function). The first step involves selecting a suitable area within the ejecta blanket of a LEC and mapping the superposed craters using the "CraterTools" (Kneissl et al., 2011), a custom tool within the ArcGIS platform. The counting area is defined as the closed area between the distal border of the continuous ejecta blankets and the inner border which is 20% crater radius away from the crater rim (Robbins and Hynek, 2012a; Lagain et al., 2020) (e.g., Fig. 3a). Due to its inherent relief (e.g., sliding slope), the erosion rate on the crater rim region is higher than that on the continuous ejecta region: the exclusion of the rim region thus could minimize the effect of resurfacing processes (Lagain et al., 2020). During the crater counting, obvious secondary craters that have irregular shapes or cluster in chains or rays were excluded to reduce overrepresentation and contamination, and the areas represented by these secondary craters were also trimmed out.

Subsequently, two individual randomness tests, i.e., standard deviation of adjacent area (SDAA) and mean 2nd-closest neighbor distance (M2CND) (Michael et al., 2012), were performed to investigate the spatial distribution and variability of craters within the measurement areas. These randomness tests provide a quantitative evaluation of the spatial distribution of the counted craters. The iteration times of the Monte Carlo simulation were set to 500 in Craterstats, and only craters that are within ±3σ of the expected value were considered for dating (e.g., the top panel in Fig. 3b shows the randomness analyses results).

Thereafter, the differential representation of the CSFD of the craters was derived and plotted using pseudo-log binning.

Finally, the AMA of the LEC was determined by fitting the CSFD to the standard martian cratering chronology. CSFD with a cumulative fitting technique is theoretically influenced and biased by the binning method in the derived model age, especially when the number of craters used to compute the CSFD is low. To constrain the unknown variables, Michael et al. (2016) introduced a Poisson timing analysis technique and expressed the dating result as a likelihood function. The Poisson timing fitting technique is preferred over binning/fitting approaches to crater-count dating in this study.

The choice of chronology system has a significant influence on the dating result, especially when the LECs in the Chryse Planitia are superposed on diverse geological units with ages ranging from the late Noachian (lN) to the early Hesperian (eH) (Fig. 2b). There are five chronology systems in the Craterstats, i.e., 'Ivanov 2001', 'Neukum-Ivanov 2001', 'Hartmann 2004 iteration', 'Hartmann & Daubar (2017)', and 'Yue et al. (2022)'. To keep with the latest chronology model that establishes the relative cratering rate between the Moon and Mars, the AMAs presented in this study are derived from the 'Yue et al. (2022)'chronology system (Yue et al., 2022) (Fig. 3b) (AMAs derived from other chronology systems are provided in the supplementary material). It should be noted that the AMA derivation in this study is performed using crater counts made on CTX mosaic (beta01 version, 5 m/pixel) (Dickson et al., 2018), thus the smallest reliable crater that can be measured is 50 m in diameter (10 pixels). However, the difference between 'Hartmann 2004 iteration' and 'Hartmann & Daubar (2017)' chronology systems is the refinement of the production function for very small craters (4 m < diameter < 45 m), the diameter range used in the present study is outside this refinement. Therefore, the AMAs derived

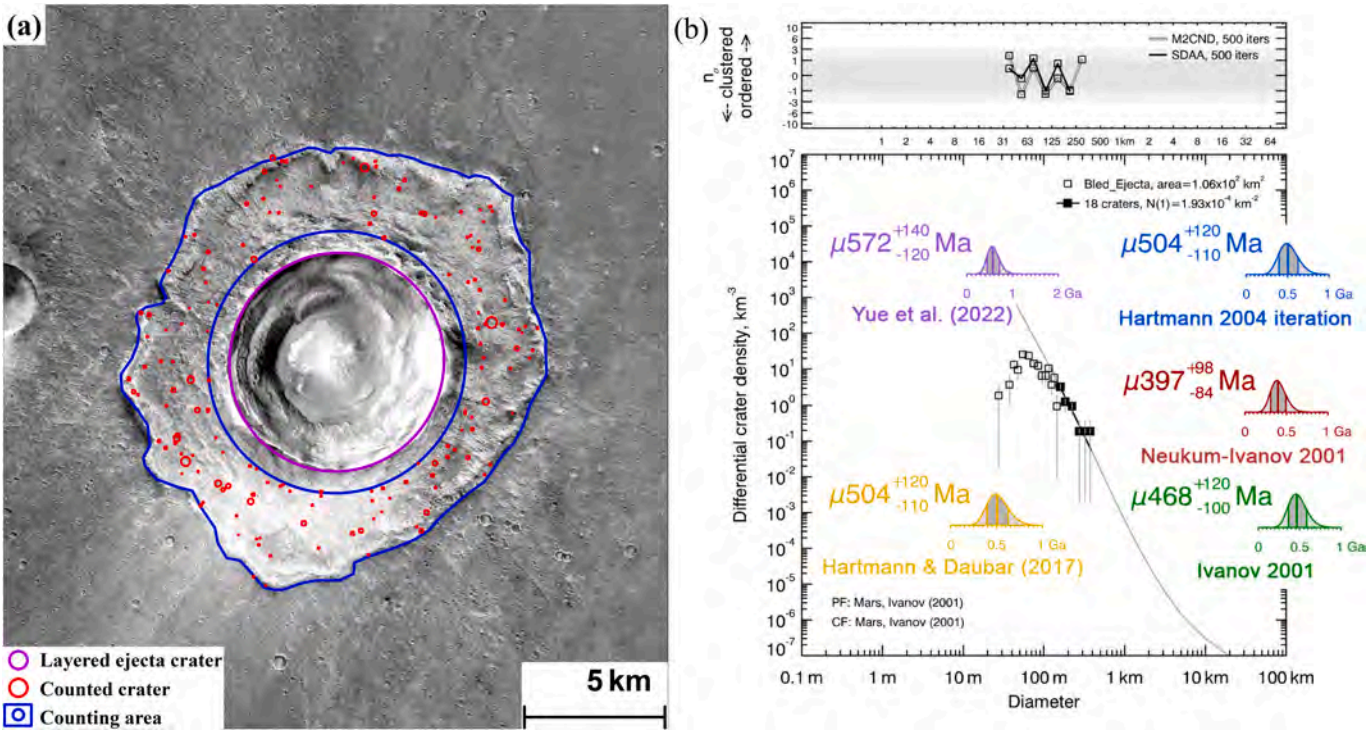

Fig. 3. (a) Bled crater in the Chryse Planitia. (b) AMAs of Bled crater based on five different chronology systems.

using these two chronologies coincide (Fig. 3b).

3.3.2. Factors considered for AMA derivation

The reliability of the AMAs derived from the CSFD method is of great importance for interpreting the paleo-environment implications of the LECs in the Chryse Planitia, i.e., the duration of the fluvial activities of the circum-Chryse outflow channels and the temporal-spatial evolution of the volatile-rich layer. Some potential shortcomings and pitfalls are considered or avoided in this study.

First, the fluidized ejecta blanket of a small LEC usually has a limited coverage area, which could potentially bias the derived model age (Warner et al., 2015; Fassett, 2016). As a result, only a LEC with a counting area >100 km^2 is considered as a candidate crater for dating.

Second, it was observed that many fluidized ejecta blankets were heavily eroded, have predominantly rugged morphologies or lack superposed craters. Consequently, to best avoid selection biases, only LECs with enough craters superposed on well-preserved or slightly eroded (if any) smooth ejecta were considered suitable for dating.

Third, the previously formed craters overlapped by the ejecta blanket of the associated large LEC were excluded from the counting pool. The most obvious examples are the Yuty crater (Supplementary Fig. 1) and the Gamboa crater (Supplementary Fig. 2).

Fourth, the rheology (physical properties) of the layered ejecta strongly influences the final crater diameter formed on top of the ejecta. As the study area is dominated by Hto and lHl units (Fig. 2b), the difference in rheology in the impacted material that controls the crater diameter and excavation depth is thought to be negligible.

In addition, many other factors may also introduce uncertainties in the dating results, e.g., the accuracy of crater diameter measurements, the existence of resurfacing process, and the statistical significance of the measured craters (Michael and Neukum, 2010; Kneissl et al., 2011; Fassett, 2016; Michael et al., 2016).

Considering the above-mentioned factors, only a quarter (25.7%, counts: 135) of the LECs were dated in this study (their locations are listed in the supplementary material). Because crater model ages and their associated statistical errors are inseparable from the crater chronology model calibration errors (Michael et al., 2016), all the AMAs derived in this study are presented with an intrinsic uncertainty preceded by the letter 'μ'.

3.4. Characterization of layered ejecta morphology

The morphologies of the layered ejecta are believed to provide information about the impact environment during ejecta emplacement (Barlow, 2004), e.g., impact angle, and impact kinetic energy. Two morphology parameters, ejecta mobility (EM) and lobateness (Γ) are calculated in this study.

Ejecta mobility (EM) characterizes the ejecta flow distance and is defined as the ratio of the average extent of the ejecta deposits out from the crater rim ($R_{ejecta\_average}$) to the crater radius (R_{crater}) (Eq. 1) (Mouginis-Mark, 1979; Barlow, 2006; Barlow and Robbins, 2015).

$$EM = \frac{R_{ejecta\_average}}{R_{crater}} = \frac{\left(\sqrt{\left(A_{ejecta} + A_{crater}\right)/\pi} - R_{crater}\right)}{R_{crater}} \quad (1)$$

Lobateness (Γ) describes the sinuosity of the ejecta flow front and is computed from the outer perimeter (P_{ejecta}) and total area (A_{ejecta}) of the ejecta deposit (Eq. 2) (Kargel, 1986; Barlow and Robbins, 2015). An ejecta deposit with $\Gamma = 1$ indicates that the ejecta is circular, and $\Gamma > 1$ implies a sinuous ejecta.

$$\Gamma = \frac{P_{ejecta}}{\sqrt{4\pi A_{ejecta}}} \quad (2)$$

3.5. Estimation of the minimal roof depth of the volatile-rich layer that fluidizes the ejecta

Experimental and numerical studies support the hypothesis that the subsurface volatile-rich layer is responsible for the formation of LECs (Woronow, 1981; Stewart et al., 2001). To form layered ejecta, the impactor must penetrate into/through the volatile-rich layer. Therefore, the depth of the upper boundary of the volatile-rich layer can be estimated from the LEC's excavation depth. The excavation depth (D_{exc}) of a crater is about one-tenth of the diameter of the transient crater (D_t) (Eq. 3) (Melosh, 1989). For a simple crater, D_t is approximately equal to the current crater's rim-to-rim diameter (D_r) (Melosh, 1989) (Eq. 3). For a complex crater, D_t is estimated from D_r using the relationship developed by Croft (1985) (Eq. 3).

$$D_{exc} \approx 0.1D_t \approx \begin{cases} 0.1D_r & D_r < D_{sc}(\text{simple crater}) \\ 0.1D_{sc}^{0.15}D_r^{0.85} & D_r \geq D_{sc}\ (\text{complex crater}) \end{cases} \quad (3)$$

where D_{sc} is the simple to complex crater transition diameter, which is ~6 km on average for martian craters (Robbins and Hynek, 2012b).

It should be noted that a given threshold fraction of volatiles (e.g., 16%–60%) is required to sufficiently fluidize the ejecta (Woronow, 1981; Stewart et al., 2001; Barlow, 2004). Therefore, below the onset diameter, the absence of fluidized ejecta does not necessarily imply an absence of volatiles in the subsurface. For example, the presence below the martian surface of one or several very thin volatile-rich layer(s) has already been observed directly by the Phoenix lander (Smith et al., 2009) and remotely by the HiRISE camera (Dundas et al., 2014; Dundas et al., 2018; Dundas et al., 2021; Dundas et al., 2023). Consequently, the depth estimated from Eq. 3 is the minimal roof depth of the volatile-rich layer to fluidize the ejecta, i.e., the approach may miss layers that have fewer volatiles for the ejecta to be fluidized.

4. Results

4.1. Distribution of LECs

A total of 525 LECs (157 of which are newly reported) were identified and catalogued in the study area (Fig. 4a). When classified by the layered ejecta patterns, the number of SLE, DLE, and MLE craters are 477 (90.9%), 29 (5.5%), and 19 (3.6%) (Fig. 4b) (the spatial distribution of each type is shown in Supplementary Fig. 3), respectively. The largest and smallest LECs are the 65 km Kipini crater (31.58°W, 25.84°N) and an unnamed 1 km crater (38.43°W, 39.37°N), respectively (Supplementary Fig. 4). Based on the morphological characteristics, 122 (23.2%) LECs can be classified as complex LECs. Among the rest 403 (76.8%) simple LECs, 191 craters are smaller than 3 km in diameter (Fig. 4d).

The onset diameter in each latitude interval decreases from 2.8 km to 1 km with increasing latitude. When compared with "uniform distribution" values (represented by the red squares in Fig. 4e), the actual distribution of LECs shows that there is a higher occurrence of LECs in the regions ≥35° N. These findings derived from the updated catalogue in this study are consistent with previous publications reporting the emplacement of craters with layered ejecta increases with higher latitudes and the onset diameter being latitude-dependent (Mouginis-Mark, 1979; Costard, 1989; Barlow and Perez, 2003; Li et al., 2015).

4.2. AMAs of LECs

Concerning the crater degradation state and counting areas, there are 135 LECs (25.7%) that are deemed valid for crater dating, including 90 SLE craters, 26 DLE craters, and 19 MLE craters (Supplementary Fig. 3). The oldest and youngest craters among these dated LECs are the eroded Concord crater ($\mu 3.72^{+0.097}_{-0.17}$ Ga; 34.02°W, 16.53°N) and the fresh Santa

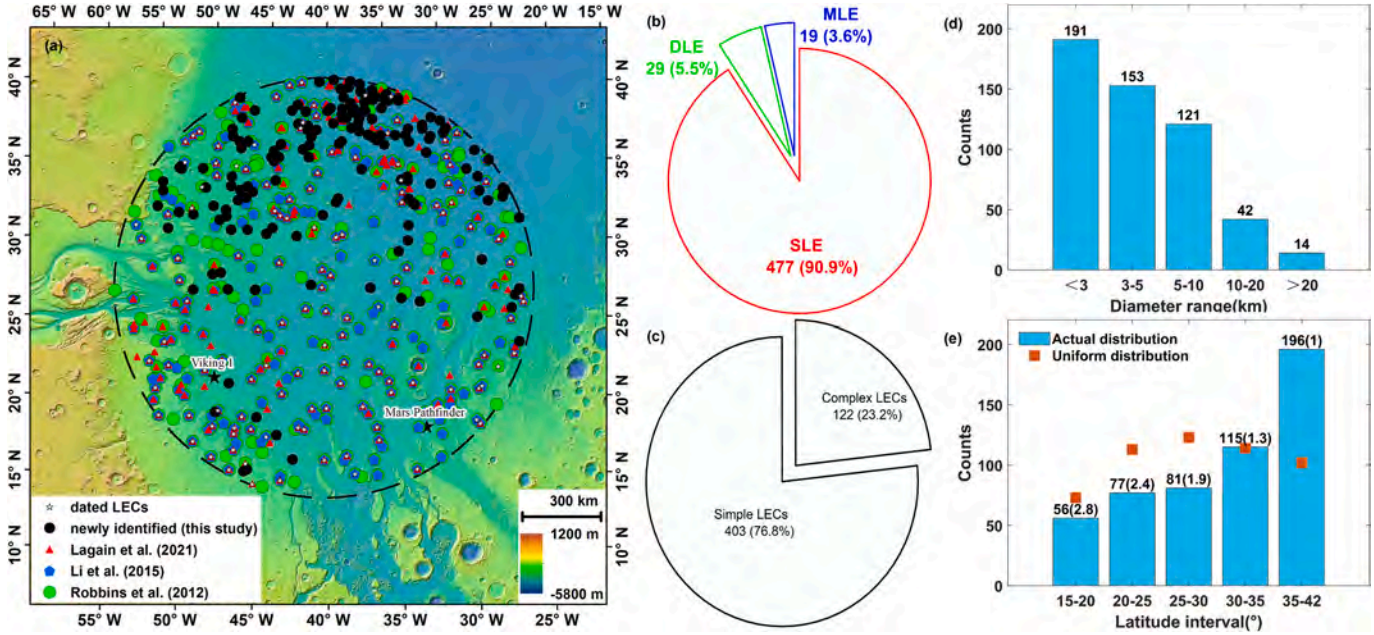

Fig. 4. (a) Identification results of the LECs; (b) Pie chart of SLE, DLE and MLE craters; (c) Pie chart of simple and complex LECs; (d) Distribution of LECs in each diameter range. The number of LECs in each range is shown on top of each bar; (e) Distribution of LECs in each latitude interval. The bars show the actual distribution of LECs in each interval, the number and onset diameter (km) of the LECs are presented on top of each bar. The red squares show the probable distribution if all the identified LECs were distributed uniformly within the study area, with the area of each latitude interval being considered. These "uniform distribution" values are calculated by multiplying the areas of each latitude interval with the average density of the LECs. (For interpretation of the references to colour in this figure legend, the reader is referred to the web version of this article.)

Fe crater ($\mu 15.8^{+1.9}_{-1.9}$ Ma; 47.94°W, 19.27°N), respectively (Supplementary Fig. 5). According to the martian epoch boundaries defined by Hartmann (2005), there are 3 LECs formed in the late Noachian (lN), 2 in the early Hesperian (eH), 2 in the late Hesperian (lH), 55 in the early Amazonian (eA), 48 in the middle Amazonian (mA), and 25 in the late Amazonian (lA) (Fig. 5) (Supplementary Table 1).

4.3. Morphologies of LECs

Among the dated LECs, a minority (counts: 10, percentage: 7.4%) of their ejecta are partially eroded or covered, thus the EM and lobateness values are calculated for the rest 125 (92.6%) LECs whose ejecta are well preserved. The EM values (Table 1) of the SLE craters range from 0.76 to 2.56, with an average value of 1.57 ± 0.33 (expressed in the form of 'mean ± standard deviation'); the EM values for the outer layer of the DLE craters range from 1.07 to 2.97, with an average value of 1.88 ± 0.48; the EM values for the outer layer of the MLE craters range from 1.15 to 3.50, with an average value of 2.07 ± 0.52. The lobateness values (Table 1) of the SLE craters range from 1.09 to 1.86, with an average value of 1.33 ± 0.16; the lobateness values for the outer layer of the DLE craters range from 1.15 to 1.77, with an average value of 1.48 ± 0.16; the lobateness values for the outer layer of the MLE craters range from 1.26 to 1.98, with an average value of 1.58 ± 0.22. Average EM values on Mars vary depending on the type of layered ejecta, typically increasing from the equator toward the poles but showing small variations among different terrains (Barlow and Robbins, 2015). The THEMIS-based research on a global scale shows that the average EM value for the SLE craters is 1.5, for the inner layer of DLE craters is 1.5, for the outer layer of DLE craters is 3.2, and for the MLE is 2.2 (Barlow, 2005). Lobateness values also vary with location and ejecta type, with an average of 1.1 for SLE, 1.0 for the inner layer of DLE, 1.1 for the outer

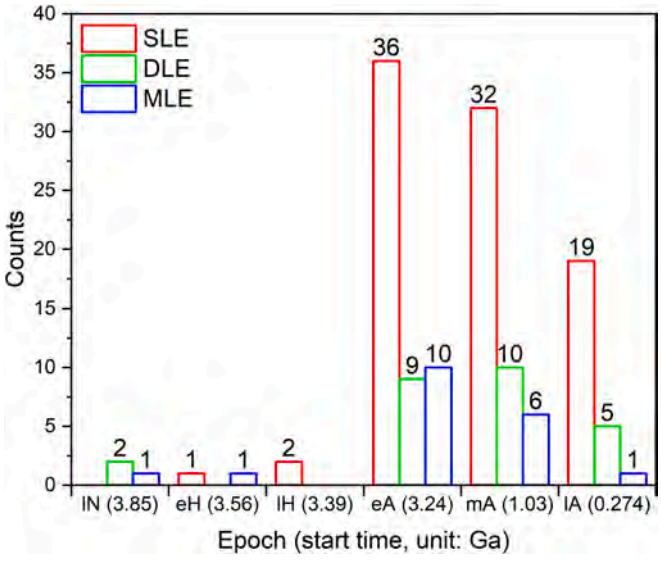

Fig. 5. Histogram of the formation epochs of different LEC types.

Table 1
Morphologies of 125 dated LECs whose ejecta are well preserved.*

Item	SLE	DLE	MLE
number	84	24	17
Diameter range (km)	4.44– 17.38	5.96– 25.75	7.97– 34.08
EM range	0.76– 2.56	1.07– 2.97	1.15– 3.50
EM median	1.55	1.75	2.08
EM mean ± standard deviation	1.57 ± 0.33	1.88 ± 0.48	2.07 ± 0.52
Lobateness range	1.09– 1.86	1.15– 1.77	1.26– 1.98
Lobateness median	1.33	1.48	1.56
Lobateness mean ± standard deviation	1.33 ± 0.16	1.48 ± 0.16	1.58 ± 0.22

* The EM and lobateness values are only calculated for the outer layer of DLE and MLE craters.

layer of DLE, and 1.2 for MLE (Barlow, 2005). The slight discrepancy between the previous study and this work is largely due to the use of the high-resolution CTX mosaic, which allows for much more accurate tracing of the ejecta boundaries.

For each type of the LECs, the average EM values increase from the low to the high latitude (Supplementary Tables 2–4, Fig. 6a), e.g., the EM value of SLE in the latitude interval of 15–20° is smaller than that in other latitude intervals. Within each latitude interval, the average EM values gradually increase with the number of layered ejecta, e.g., in the 20–25° latitude interval, the average EM values of the SLE, DLE, and MLE are 1.37, 1.65, and 1.81, respectively. Because the runout distance of the ejecta relies on many factors (e.g., surface roughness, volatile abundance, impact angle and velocity), the estimation of the amount of mobilized volatile material during impacts from EM values is not a straightforward process. The lobateness values of the SLE craters have a decreasing trend with increasing latitude (Fig. 6b), however, such a trend is not obvious for the DLE and MLE craters. The decreasing trend of the lobateness vs latitude shown here could be due to an increasing erosion rate at higher latitudes (Thomson, 2018). These observations are consistent with those from previous studies that investigated the parameters at a global scale (Barlow, 2005; Barlow and Robbins, 2015).

4.4. Excavation depth of LECs

The excavation depths of the 135 dated LECs are estimated (Eq. 3), giving values mostly between 500 and 1000 m (Fig. 7a). Larger impacts excavate deeper voids and the resulting craters have a longer survival expectancy. The average diameters of DLE craters and MLE craters dated in this study are larger than that of the SLE craters (the histogram of diameter ranges of different LECs are shown in Supplementary Fig. 6), therefore, there is a clear trend showing that DLE and MLE craters exhume deeper materials than SLE craters (Fig. 7b). The shallowest excavation depths of the dated SLE, DLE, and MLE craters are 440 m, 600 m, and 760 m, respectively, and the average excavation depths of the SLE, DLE, and MLE craters are 781 ± 240 m, 1128 ± 445 m, and 1563 ± 626 m, respectively (Fig. 7b) (Supplementary Table 5).

5. Discussions

5.1. Constraints on the timing of the circum-Chryse fluvial activities

During the identification of LECs, it was observed that some LECs were clearly eroded by fluvial processes, and some were superposed either on the valley channels (Fig. 8) or the surrounding terra. Therefore, when the AMAs of the LECs are determined, the spatial superposition relationship between the LECs and the fluvial features becomes a useful indicator to constrain the duration of the circum-Chryse fluvial activities.

5.1.1. Ares Vallis, Tiu Valles and Simud Valles

The Ares Vallis (center location: 25.61°W, 10.29°N) is one of the largest circum-Chryse outflow channels and was produced by multiple time-scattered events, including catastrophic flooding, glacial, and periglacial processes (Pacifici et al., 2009; Warner et al., 2009). The floor of the main Ares Vallis channel is generally ~150 m to 2000 m below the adjacent highly incised Noachian highlands (Warner et al., 2009; Tanaka et al., 2014). In the Ares Vallis, the LECs with partially eroded ejecta by fluvial activities have AMAs between $\mu 3.72^{+0.097}_{-0.17}$ Ga (Concord crater in Fig. 8a and Fig. 9a-b) and $\mu 2.79^{+0.25}_{-0.34}$ Ga (Zuni crater in Fig. 8b and Fig. 9a-b), suggesting the water flows that carved the channels and eroded the ejecta occurred between the late Noachian (lN) and early Amazonian (eA).

The Tiu Valles (center location: 34.86°W, 16.23°N) and Simud Valles (center location: 38.01°W, 19.09°N), both cross-cutting the Ares Vallis, were also shaped by catastrophic floods and were carved by episodic volcanic and fluvial/glacial geologic activities (Neukum et al., 2010). There are LECs eroded by fluvial processes in the Tiu and Simud Valles, however, their ejecta blankets experienced severe degradation, e.g., the Luck crater (location: 36.91°W, 17.26°N; diameter: 8 km). The small counting area and the high degradation state make any AMA derivation impossible to perform for these heavily eroded craters. Dating results for craters with ejecta blankets superposed on the valley channels have AMAs younger than $\mu 2.65^{+0.48}_{-0.62}$ Ga (Warra crater in Fig. 8c and Fig. 9a-b), suggesting the fluvial activities in the Tiu and Simud Valles ceased during the early Amazonian before ~ μ2.7 Ga.

These constraints on the fluvial activities for the Ares Vallis, the Tiu and Simud Valles, are broadly consistent with previous studies that determined the channel floor ages. For example, Neukum and Hiller (1981) inferred the fluvial activities of Ares Vallis took place during the Hesperian. Warner et al. (2009) also found that the flooding at Ares Vallis initiated on the highest topographically lower regions during the early Hesperian (eH), and continued to modify craters in the topographically lowest into the early Amazonian. Marchenko et al. (1998) proposed that the fluvial activities of Tiu and Simud Valles occurred during the late Hesperian and might have continued into the middle Amazonian (mA).

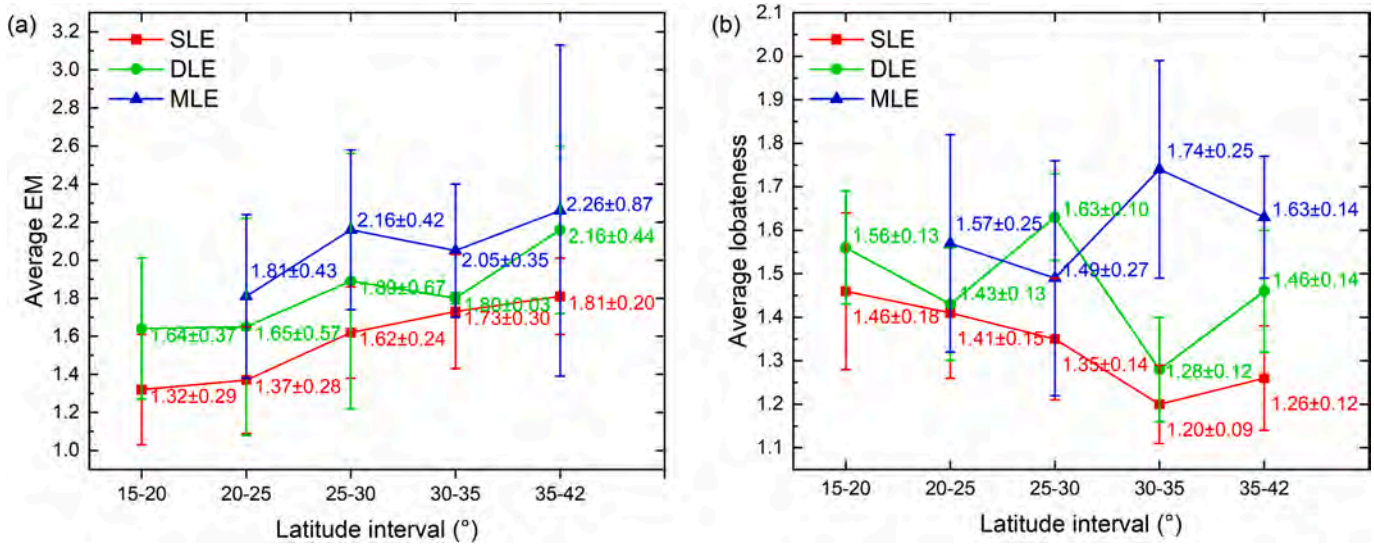

Fig. 6. EM and lobateness values at each latitude interval.

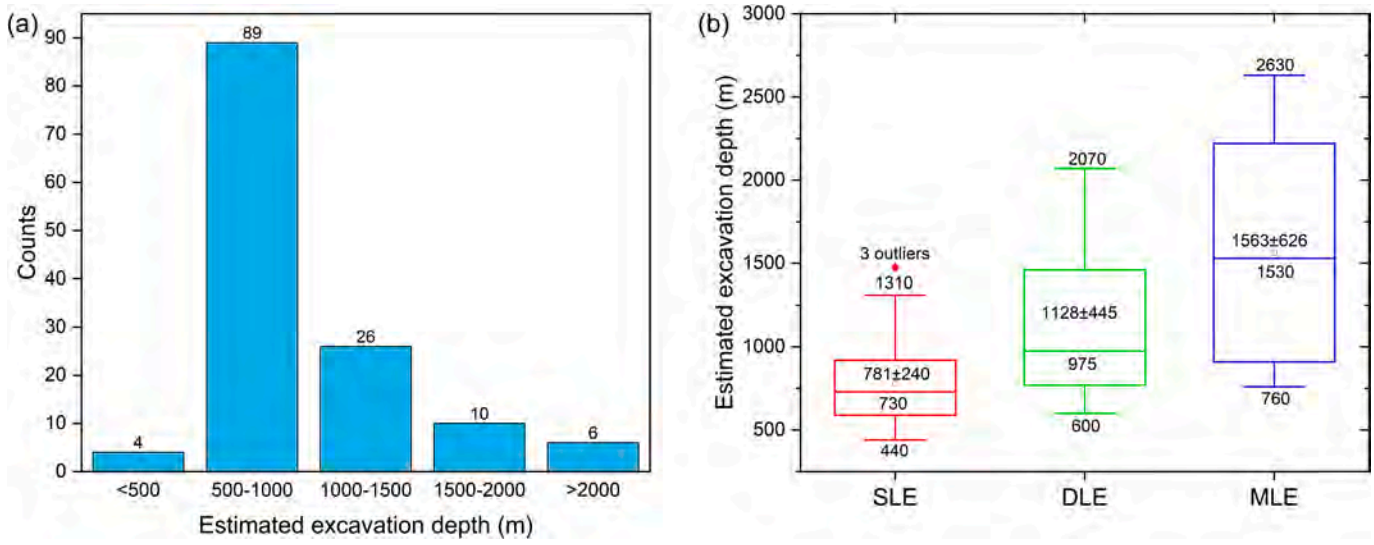

Fig. 7. (a) Distribution of estimated excavation depth. (b). Boxplot of estimated excavation depths of different types of LECs.

5.1.2. Vedra, Maumee, and Maja Valles

Three separate channel systems, Vedra Valles (center location: 55.48°W, 19.12°N), Maumee Valles (center location: 52.85°W, 19.51°N), and Maja Valles (center location: 58.38°W, 10.23°N), scoured the Hesperian Lunae Planum and debouched into the Chryse Planitia (Fig. 9c). It is evident that flows from the Vedra and Maumee Valles converged to cut the Maja Valles, whose lower ends are marked by faint alluvial fans that are cut by numerous, small, divergent channels (de Hon, 1987). LECs with partially eroded ejecta by fluvial activities show AMAs of $\mu 2.70^{+0.42}_{-0.54}$ Ga (Dromore crater in Fig. 8d and Fig. 9c)) and $\mu 2.18^{+0.53}_{-0.51}$ Ga (Weert crater in Fig. 8e and Fig. 9c), and the oldest LEC superposed on the valley channels is the $\mu 1.86^{+0.29}_{-0.29}$ (Peixe crater in Fig. 8f and Fig. 9c). The spatial superposition relationship and the derived AMAs indicate the flows that incised the Maja Valles continued into the early Amazonian and perhaps came to a halt between ~ μ2.2 Ga and ~ μ1.9 Ga.

5.1.3. Kasei Valles

The water that carved the Kasei Valles (center location: 65.0° W, 24.6° N) flowed eastward through the Lunae Planum and emptied into the Chryse Planitia (Fig. 9d). It is the largest outflow channel system on Mars and shows evidence of episodic reoccurrence of both volcanic and fluvial processes, with ice and/or floods likely responsible for carving out most of the west-to-east channels (Neukum et al., 2010). Due to a series of ancient mega-floods that shaped the Kasei Valles, almost all the LECs formed before the floods were obliterated by erosive forces, leaving only a very few heavily eroded LECs unsuitable for crater dating, e.g., Worcester (Fig. 8g) and Wassamu (Fig. 8h) craters. Among the LECs that superposed on the fluvial features in the Kasei Valles, the Guaymas crater (Fig. 8i and Fig. 9d) with an AMA of $\mu 2.80^{+0.53}_{-0.82}$ Ga is the oldest, suggesting that the resurfacing events caused by episodic fluvial activities likely ended before ~ μ2.8 Ga in the early Amazonian.

5.1.4. Paleoenvironmental conditions during Amazonian

The martian climate in the Amazonian period is usually thought to be similar to the current cold and arid conditions, however, the superposition relationship between the LECs and circum-Chryse channels suggests that the fluvial activity might have extended into the early Amazonian (the discussion of the water source is beyond the scope of this paper). Evidence of Amazonian-aged aqueous and/or glacial activities also have been reported in other regions, indicating that the martian climate during the Amazonian period was more diverse than previously thought, i.e., the possible existence of local and limited climate conditions supporting the aqueous and/or glacial activities. For example, after analysis of the jarosite at the Meridiani Planum, and the goethite and hematite in the Gusev crater that were discovered by the Opportunity and Spirit rovers, Fairén et al. (2009) proposed the presence of minor amounts of shallow acidic liquid water at local scales during the Amazonian period. Chen et al. (2015) suggested that the pre-impact aqueous-alteration products in the fresh Tissint meteorite (~600 Ma old), whose potential source might be the Tooting crater at ~23° N in the northern lowlands (Lagain et al., 2021a), could be diagnostic chemical evidence for subsurface water. Adeli et al. (2016) observed a well-preserved early to middle Amazonian-aged complex fluvial system in the Terra Cimmeria, with ice/snow melt as the water source for the surface runoff. The Zhurong rover at Utopia Planitia also found mineralogy evidence (i.e., hydrated sulfate/silica materials that are associated with locally developed duricrust) for an active aqueous Amazonian hydrosphere (Liu et al., 2022).

5.2. Implications for the temporal-spatial evolution of the subsurface volatile-rich layer

Among the dated 135 LECs in this study, 128 LECs (94.8%) were formed in the Amazonian, and the remaining 7 LECs that formed in the Hesperian and Noachian are usually large complex craters with multiple layered ejecta, e.g., Concord (20.2 km, $\mu 3.72^{+0.097}_{-0.17}$ Ga) and Libertad (31.2 km, $\mu 3.47^{+0.095}_{-0.20}$ Ga) (Table S2 in the supplementary). Large craters have a greater probability of being preserved than small craters since the latter have a shorter lifespan (relatively shallower excavation depth and low profiles). According to the relationship between excavation depth and final crater diameter (Eq. 3), the inclusion of large LECs would suggest that the minimal roof depth of the volatile-rich layer ought to be large. To eliminate the potential bias from large LECs, this study limits the analysis to 25 LECs with a diameter <6 km (transition diameter) to study the temporal and spatial variation of the volatile-rich layer in the Chryse Planitia.

Many of these 25 LECs have EM values between 1.4– 1.8 (Fig. 10a-b), have lobateness values of 1.1– 1.4 (Fig. 10c-d) and excavation depths of 560– 590 m (Fig. 10e-f). The EM value is sometimes considered as an indicator of the abundance of volatiles in the subsurface at the time of crater formation. It is probably accurate that ejecta may extend further from the crater rim if it is highly fluidized by the abundant volatiles; however, there will almost certainly be differences caused by the roughness of the pre-existing surface and the size distribution of clasts within the ejecta. This in turn would vary depending upon the crater

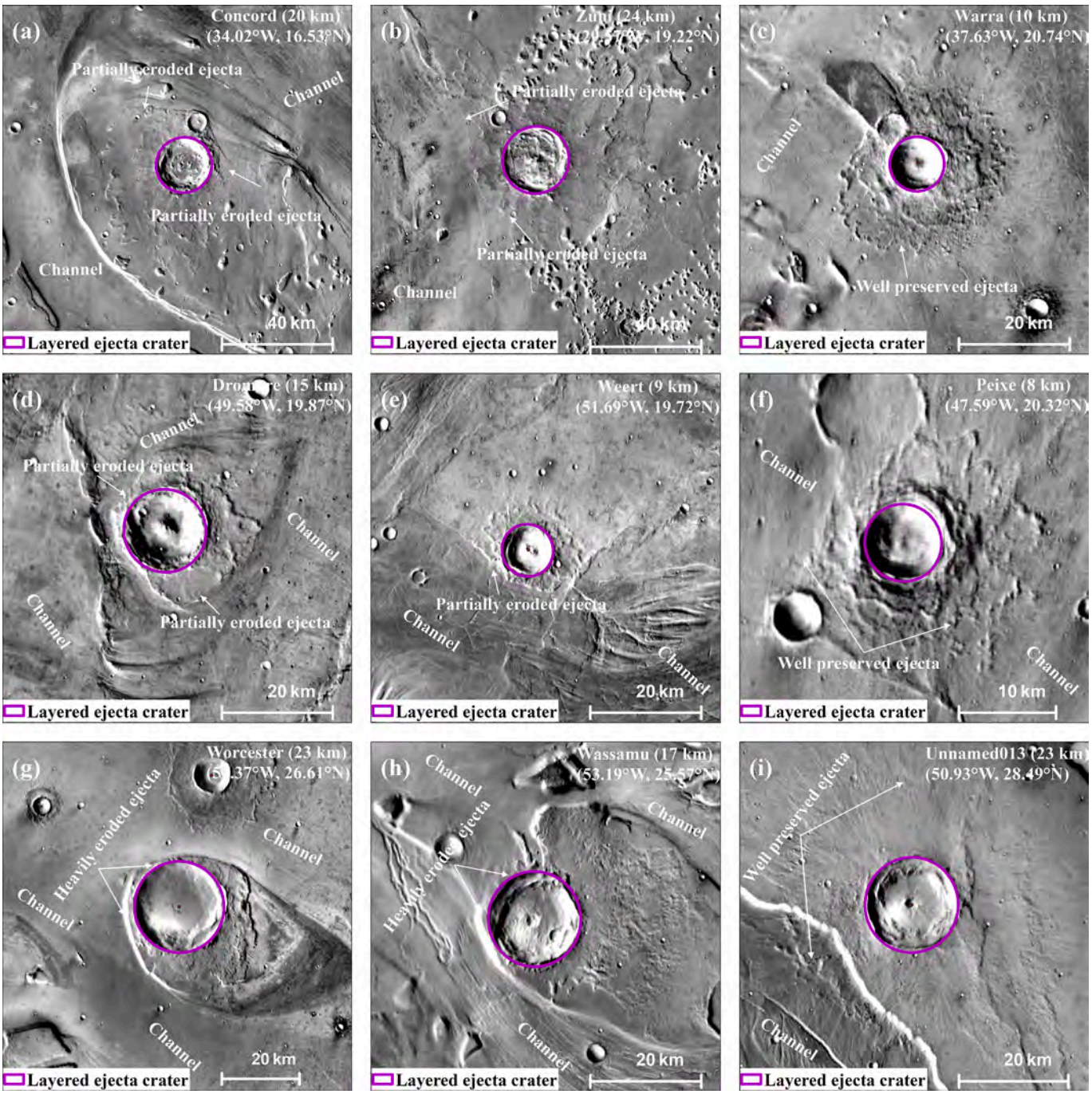

Fig. 8. Different relations of LECs and valley systems. (a, b, d, e, g, h) LECs being eroded by fluvial activities; (c, f, i) LECs superposed on the valley channels. (a)-(c) show LECs in the Ares Vallis, Tiu Valles and Simud Valles. (d-f) show LECs in the Vedra, Maumee, and Maja Valles. (g)-(i) show LECs in the Kasei Valles. The basemap is the THEMIS mosaic (Edwards et al., 2011).

being excavated within a rigid surface (e.g., coherent lavas) or unconsolidated sediments (e.g., volcanic ashes, aeolian deposits), and the angle of impact and velocity. Thus, there are potential issues in using the EM values to infer the abundance of subsurface volatiles. Therefore, the abundance of volatiles in the subsurface is not considered in this study.

Many sites on Mars are known to feature water ice just below the surface, ranging from a few centimeters (Smith et al., 2009) to decimeters (Byrne et al., 2009). Studies revealed that ice sheets in some locations at martian mid-latitudes extend downward from depths as shallow as 1 to 2 m below the surface to a depth of 100 m or even deeper (Dundas et al., 2014; Dundas et al., 2018; Dundas et al., 2021; Dundas et al., 2023). Although the depth of the volatile-rich layer varies in different locations, these findings point to the existence of volatile-rich layer(s) in the martian subsurface, which might extend on a global scale. Using principal component (PC) analysis on the LECs' morphometries, Jones (2015) identified an index of subsurface volatiles (PC2 in the study), which shows a strong latitudinal trend with higher values toward the poles. Jones (2015) interpreted this index as an indicator of a volatile-rich and potentially ice-rich target material. The index is low in the Chryse Planitia, suggesting that the present-day shallow volatiles in this region are relatively poor.

The lower part of the scatter plot of AMAs of LECs versus estimated excavation depth could be considered as defining the minimal roof depth where a sufficient fraction of volatiles was excavated. However,

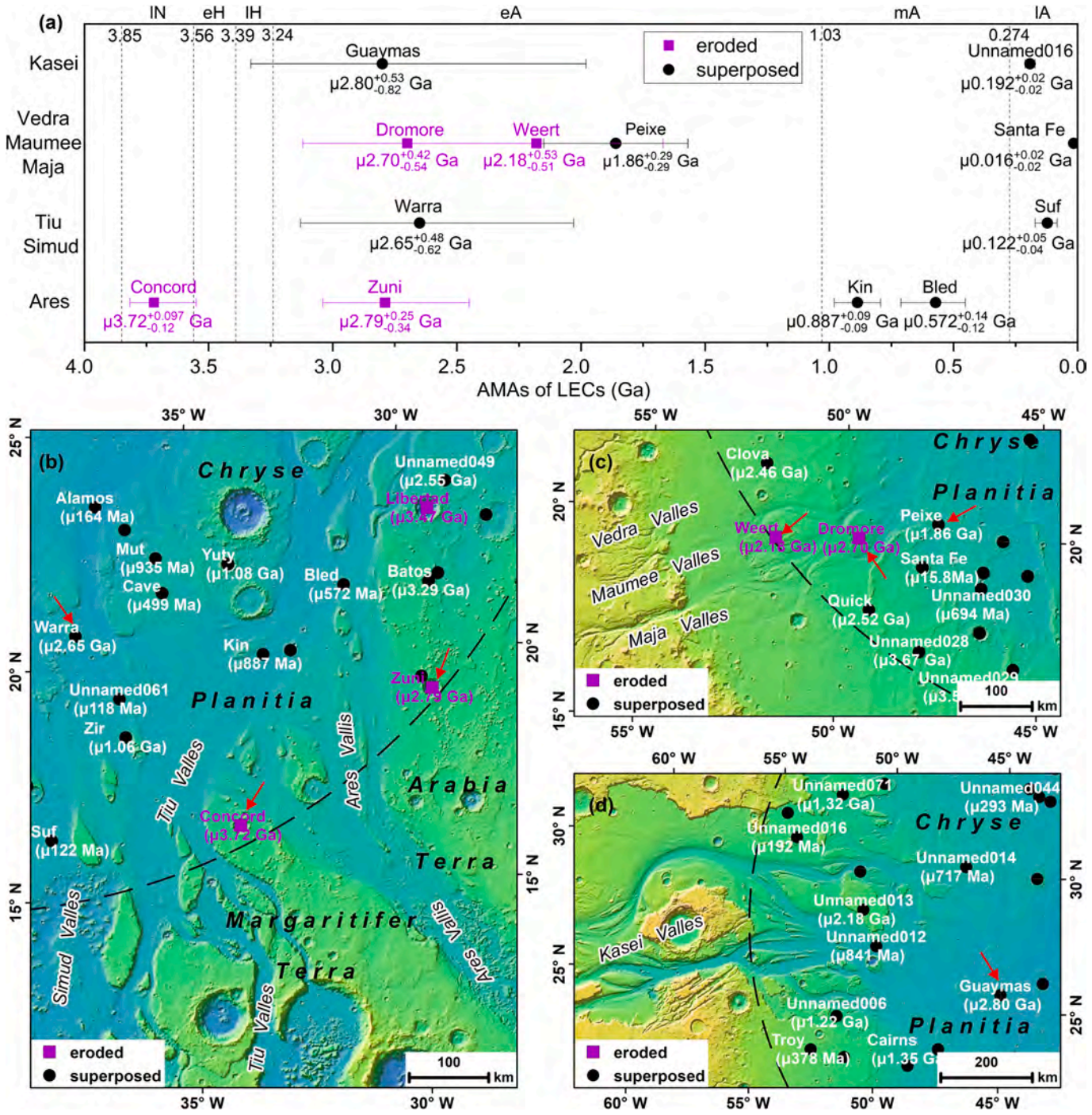

Fig. 9. (a) Summation of the minimum and maximum AMAs for different Valles. (b) LECs in the Ares Vallis, Tiu Valles and Simud Valles. (c) LECs in the Vedra Valles, Maumee Valles, and Maja Valles. (d) LECs in the Kasei Valles. The red arrows in b-d mark the locations referred to in the text. (For interpretation of the references to colour in this figure legend, the reader is referred to the web version of this article.)

the AMAs of the craters with onset diameter cannot be determined due to limited counting area. Therefore, the dated LECs with the smallest diameter in each latitude interval are used to infer the spatial variation of the minimal roof depth in this study (Fig. 11). These five LECs were formed in the Amazonian, their EM values are relatively large at latitudes >30°, and lobateness values decrease with increasing latitudes. As discussed in Section 4.3 and the above paragraph, the large EM values are not suitable for inferring the abundance of the volatiles, and small lobateness values at high latitudes might be due to increasing erosion rates at higher latitudes.

Although there is a possibility that the volatile-rich layer might migrate toward deeper or shallower regions for a short time, the dating results (Fig. 5) and the histogram (Fig. 10f) support the idea that on the geological time scale, the minimal roof depth of the volatile-rich layer has remained relatively stable at least around 560– 590 m since the early Amazonian. It is observed that the minimal roof depth has a slight difference between high and low latitudes (Fig. 11), suggestive that the minimal roof depth of the volatile-rich layer might be as shallow as ~440 m in the high latitudes and ~ 540 m in the low latitudes.

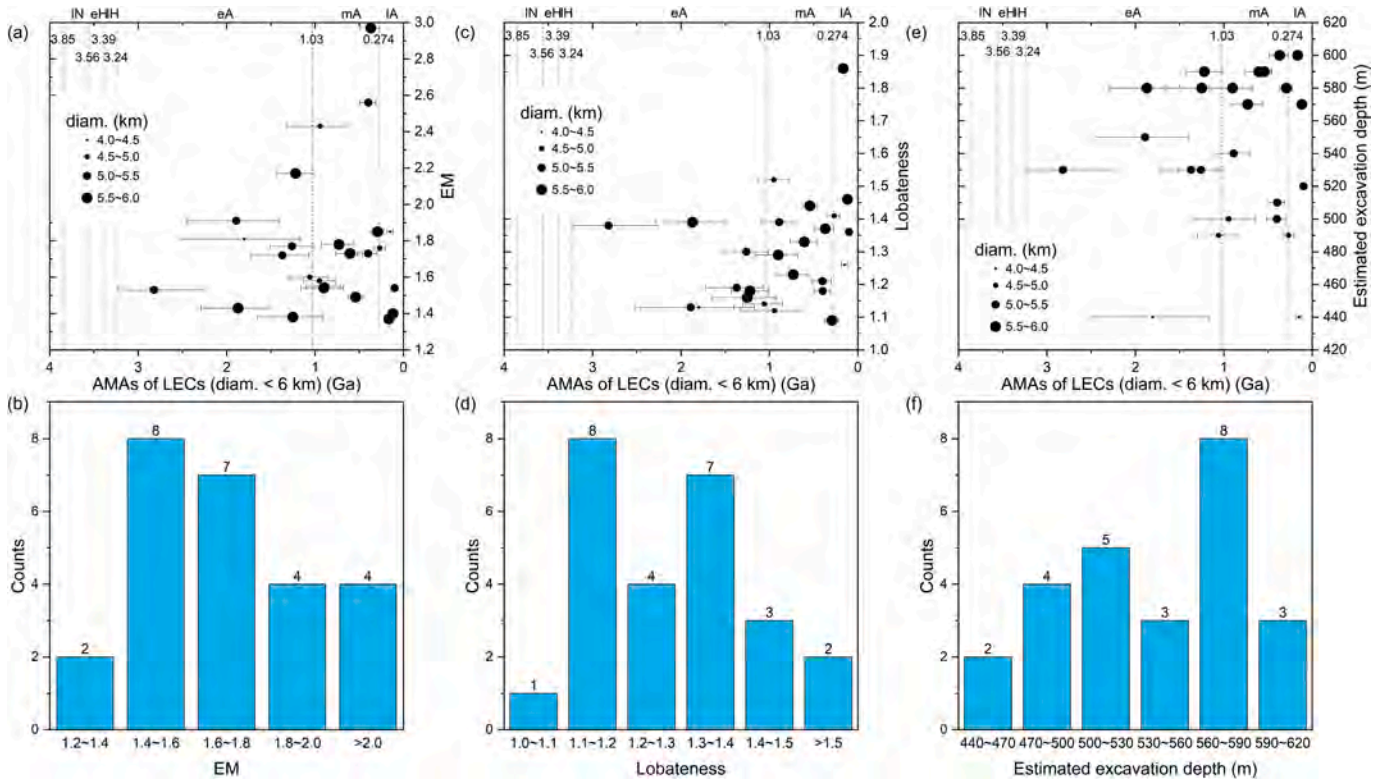

Fig. 10. (a) Scatter plot of AMAs of LECs (diam. < 6 km) versus EM values. (b) Histogram of EM values. (c) Scatter plot of AMAs of LECs (diam. < 6 km) versus lobateness values. (d) Histogram of lobateness values. (e) Scatter plot of AMAs of LECs (diam. < 6 km) versus estimated excavation depth. (f) Histogram of estimated excavation depth. The scatter plots of AMAs of different types of LECs versus EM, lobateness, and estimated excavation depth are shown in Supplementary Fig. 7.

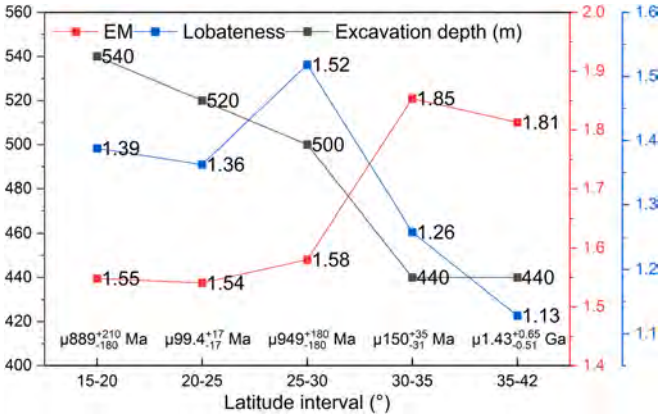

Fig. 11. EM, lobateness, estimated excavation depth, and AMA of the dated LECs with the minimum diameter at each latitude interval.

6. Conclusions

With the high resolution (5 m/pixel) CTX mosaic serving as a base map, a total of 525 LECs within the Chryse Planitia were identified and catalogued, with 157 being newly reported. When classified by the number of layered ejecta, the counts of SLE, DLE, and MLE craters are 477 (90.9%), 29 (5.5%), and 19 (3.6%), respectively. The counts of simple and complex LECs are 403 (76.8%) and 122 (23.2%), respectively. The onset diameter decreases from 2.8 km to 1 km with increasing latitudes, and a higher occurrence of LECs is observed in the regions ≥35° N.

Considering the crater degradation state and counting area, the AMAs of 135 LECs were determined (Fig. 5) to investigate their paleoenvironment implications. Although the circum-Chryse fluvial activities were still active during the early Amazonian, the water flows that scoured the Ares, Tiu, and Simud Valles might have come to a halt before ~ μ2.7 Ga, the erosion on the channels of the Vedra Valles, Maumee Valles, and Maja Valles might stop between ~μ2.2 Ga and ~ μ1.9 Ga, and the episodic fluvial events in the Kasei Valles might have ended earlier than ~μ2.8 Ga.

It is plausible that the volatile-rich layer might have experienced a migration toward deeper or shallower regions for a short time. However, the high number of LECs formed in the Amazonian (128 LECs, 94.8%, Fig. 5) and the excavation depths of LECs with diameter <6 km (Fig. 10 e-f) support the hypothesis that, on a geological time scale, the minimal roof depth of the subsurface volatile-rich layer has remained relatively stable at least around 560– 590 m since the early Amazonian, and it is perhaps as shallow as ~440 m in the high latitudes and ~540 m in the low latitudes.

Declaration of Competing Interest

The authors declare that they have no known competing financial interests or personal relationships that could have appeared to influence the work reported in this article.

Data availability

The authors have uploaded data as supplementary material

Acknowledgements

This research is supported by the National Key Research and Development Program of China (Grant No. 2021YFA0716100), Strategic Priority Research Program of the Chinese Academy of Sciences (grant No. XDB41000000), National Natural Science Foundation of China (Grant Nos. 42172265 and 42241111), Macao Young Scholars Program

(grant No. AM201902), and the Key Research Program of the Institute of Geology and Geophysics, Chinese Academy of Sciences (grant No. IGGCAS-202204). The CTX mosaic used in this work was downloaded from the Bruce Murray Laboratory for Planetary Visualization (http://murray-lab.caltech.edu/CTX/). The locations of the identified 525 LECs, shapefiles of both the counting area and counted craters, the spatial crater count (SCC) files and dating results of the 135 LECs are available in the supplementary material. The authors greatly thank Dr. Anthony Lagain and an anonymous reviewer for their insightful reviews that improved the quality of the manuscript substantially, and Dr. Christina Viviano for editorial handling.

Appendix A. Supplementary data

Supplementary data to this article can be found online at https://doi.org/10.1016/j.icarus.2023.115918.

References

Adeli, S., Hauber, E., Kleinhans, M., Le Deit, L., Platz, T., Fawdon, P., Jaumann, R., 2016. Amazonian-aged fluvial system and associated ice-related features in Terra Cimmeria. Mars. Icarus. 277, 286–299.
Barlow, N.G., 2004. Martian subsurface volatile concentrations as a function of time: clues from layered ejecta craters. Geophys. Res. Lett. 31 (5), L05703.
Barlow, N.G., 2005. A review of Martian impact crater ejecta structures and their implications for target properties. In: Kenkmann, T., Hörz, F., Deutsch, A. (Eds.), Large Meteorite Impacts III, 384. Geological Society of America Special Paper, pp. 433–442.
Barlow, N.G., 2006. Impact craters in the northern hemisphere of Mars: layered ejecta and central pit characteristics. Meteoritics & Planetary Science. 41, 1425–1436.
Barlow, N., 2015. Characteristics of impact craters in the northern hemisphere of Mars. In: Osinski, G.R., Kring, D.A. (Eds.), Large Meteorite Impacts and Planetary Evolution V, Geological Society of America Special Paper, vol. 518, pp. 31–63.
Barlow, N.G., Bradley, T.L., 1990. Martian impact craters: correlations of ejecta and interior morphologies with diameter, latitude, and terrain. Icarus. 87 (1), 156–179.
Barlow, N.G., Perez, C.B., 2003. Martian impact crater ejecta morphologies as indicators of the distribution of subsurface volatiles. Journal of Geophysical Research: Planets. 108 (E8), 5085.
Barlow, N.G., Robbins, S., 2015. Layered ejecta. In: Hargitai, H., Kereszturi, Á. (Eds.), Encyclopedia of Planetary Landforms. Springer, New York, New York, NY, pp. 1192–1197.
Barlow, N.G., Boyce, J.M., Costard, F.M., Craddock, R.A., Garvin, J.B., Sakimoto, S.E.H., Kuzmin, R.O., Roddy, D.J., Soderblom, L.A., 2000. Standardizing the nomenclature of Martian impact crater ejecta morphologies. Journal of Geophysical Research: Planets. 105 (E11), 26733–26738.
Barlow, N.G., Koroshetz, J., Dohm, J.M., 2001. Variations in the onset diameter for Martian layered ejecta morphologies and their implications for subsurface volatile reservoirs. Geophys. Res. Lett. 28 (16), 3095–3098.
Barnouin-Jha, O.S., Schultz, P.H., 1998. Lobateness of impact ejecta deposits from atmospheric interactions. Journal of Geophysical Research: Planets. 103 (E11), 25739–25756.
Boyce, J., Barlow, N., Mouginis-Mark, P., Stewart, S., 2010. Rampart craters on Ganymede: their implications for fluidized ejecta emplacement. Meteoritics & Planetary Science. 45 (4), 638–661.
Byrne, S., Dundas, C.M., Kennedy, M.R., Mellon, M.T., McEwen, A.S., Cull, S.C., Daubar, I.J., Shean, D.E., Seelos, K.D., Murchie, S.L., Cantor, B.A., Arvidson, R.E., Edgett, K.S., Reufer, A., Thomas, N., Harrison, T.N., Posiolova, L.V., Seelos, F.P., 2009. Distribution of mid-latitude ground ice on Mars from new impact craters. Science. 325 (5948), 1674–1676.
Carr, M.H., Head, J.W., 2010. Geologic history of Mars. Earth Planet. Sci. Lett. 294 (3), 185–203.
Carr, M.H., Crumpler, L.S., Cutts, J.A., Greeley, R., Guest, J.E., Masursky, H., 1977. Martian impact craters and emplacement of ejecta by surface flow. J. Geophys. Res. 82 (28), 4055–4065.
Chen, Y., Liu, Y., Guan, Y., Eiler, J.M., Ma, C., Rossman, G.R., Taylor, L.A., 2015. Evidence in Tissint for recent subsurface water on Mars. Earth Planet. Sci. Lett. 425, 55–63.
Costard, F.M., 1989. The spatial distribution of volatiles in the Martian hydrolithosphere. Earth Moon Planet. 45 (3), 265–290.
Croft, S.K., 1985. The scaling of complex craters. J. Geophys. Res. Solid Earth 90 (S02), C828–C842.
de Hon, R.A., 1987. Eastern Lunae Planum outflow complex: Analogy to overbank flooding. In: 18th Lunar and Planetary Science Conference. Houston, Texas, pp. 227–228.
Dickson, J.L., Kerber, L.A., Fassett, C.I., Ehlmann, B.L., 2018. A global, blended CTX mosaic of Mars with Vectorized seam mapping: A new mosaicking pipeline using principles of non-destructive image editing. In: In: 49th Lunar and Planetary Science Conference. The Woodlands, Texas, p. 2480.
Dundas, C.M., Byrne, S., McEwen, A.S., Mellon, M.T., Kennedy, M.R., Daubar, I.J., Saper, L., 2014. HiRISE observations of new impact craters exposing Martian ground ice. Journal of Geophysical Research: Planets. 119 (1), 109–127.
Dundas, C.M., Bramson, A.M., Ojha, L., Wray, J.J., Mellon, M.T., Byrne, S., McEwen, A.S., Putzig, N.E., Viola, D., Sutton, S., Clark, E., Holt, J.W., 2018. Exposed subsurface ice sheets in the Martian mid-latitudes. Science. 359 (6372), 199–201.
Dundas, C.M., Mellon, M.T., Conway, S.J., Daubar, I.J., Williams, K.E., Ojha, L., Wray, J. J., Bramson, A.M., Byrne, S., McEwen, A.S., Posiolova, L.V., Speth, G., Viola, D., Landis, M.E., Morgan, G.A., Pathare, A.V., 2021. Widespread exposures of extensive clean shallow ice in the Midlatitudes of Mars. Journal of Geophysical Research: Planets. 126 (3) (e2020JE006617).
Dundas, C.M., Mellon, M.T., Posiolova, L.V., Miljković, K., Collins, G.S., Tornabene, L.L., Rangarajan, V.G., Golombek, M.P., Warner, N.H., Daubar, I.J., Byrne, S., McEwen, A. S., Seelos, K.D., Viola, D., Bramson, A.M., Speth, G., 2023. A large new crater exposes the limits of water ice on Mars. Geophys. Res. Lett. 50 (2) (e2022GL100747).
Edwards, C., Nowicki, K., Christensen, P., Hill, J., Gorelick, N., Murray, K., 2011. Mosaicking of global planetary image datasets: 1. Techniques and data processing for thermal emission imaging system (THEMIS) multi-spectral data. J. Geophys. Res. 116 (E10), E10008.
Fairén, A.G., Schulze-Makuch, D., Rodríguez, A.P., Fink, W., Davila, A.F., Uceda, E.R., Furfaro, R., Amils, R., McKay, C.P., 2009. Evidence for Amazonian acidic liquid water on Mars—a reinterpretation of MER mission results. Planet. Space Sci. 57 (3), 276–287.
Fassett, C.I., 2016. Analysis of impact crater populations and the geochronology of planetary surfaces in the inner solar system. Journal of Geophysical Research: Planets. 121 (10), 1900–1926.
Golombek, M.P., Cook, R.A., Economou, T., Folkner, W.M., Haldemann, A.F.C., Kallemeyn, P.H., Knudsen, J.M., Manning, R.M., Moore, H.J., Parker, T.J., Rieder, R., Schofield, J.T., Smith, P.H., Vaughan, R.M., 1997. Overview of the Mars pathfinder Mission and assessment of landing site predictions. Science. 278 (5344), 1743–1748.
Hartmann, W.K., 2005. Martian cratering 8: Isochron refinement and the chronology of Mars. Icarus. 174 (2), 294–320.
Hughson, K.H.G., Russell, C.T., Schmidt, B.E., Chilton, H.T., Sizemore, H.G., Schenk, P. M., Raymond, C.A., 2019. Fluidized appearing ejecta on Ceres: implications for the mechanical properties, frictional properties, and composition of its shallow subsurface. Journal of Geophysical Research: Planets. 124 (7), 1819–1839.
Jones, E., 2015. Identifying an index of subsurface volatiles on Mars through an analysis of impact crater morphometry using principal component analysis. Journal of Geophysical Research: Planets. 120 (12), 2084–2101.
Jones, E., Osinski, G.R., 2015. Using martian single and double layered ejecta craters to probe subsurface stratigraphy. Icarus. 247, 260–278.
Kadish, S.J., Head, J.W., 2014. The ages of pedestal craters on Mars: evidence for a late-Amazonian extended period of episodic emplacement of decameters-thick mid-latitude ice deposits. Planet. Space Sci. 91, 91–100.
Kargel, J.S., 1986. Morphologic variations of Martian rampart crater ejecta and their dependencies and implications. In: 17th Lunar and Planetary Science Conference. Houston, Texas, pp. 410–411.
Kneissl, T., van Gasselt, S., Neukum, G., 2011. Map-projection-independent crater size-frequency determination in GIS environments—new software tool for ArcGIS. Planet. Space Sci. 59 (11), 1243–1254.
Komatsu, G., Ori, G.G., Di Lorenzo, S., Rossi, A.P., Neukum, G., 2007. Combinations of processes responsible for Martian impact crater "layered ejecta structures" emplacement. Journal of Geophysical Research: Planets. 112, E06005.
Kuzmin, R.O., Bobina, N.N., Zabalueva, E.V., Shashkina, V.P., 1988. Inhomogeneities in the upper levels of the Martian Cryolithosphere. In: 19th Lunar and Planetary Science Conference. Houston, Texas, pp. 655–656.
Lagain, A., Bouley, S., Baratoux, D., Costard, F., Wieczorek, M., 2020. Impact cratering rate consistency test from ages of layered ejecta on Mars. Planet. Space Sci. 180, 104755.
Lagain, A., Benedix, G.K., Servis, K., Baratoux, D., Doucet, L.S., Rajšic, A., Devillepoix, H. A.R., Bland, P.A., Towner, M.C., Sansom, E.K., Miljković, K., 2021a. The Tharsis mantle source of depleted shergottites revealed by 90 million impact craters. Nat. Commun. 12 (1), 6352.
Lagain, A., Bouley, S., Baratoux, D., Marmo, C., Costard, F., Delaa, O., Pio Rossi, A., Minin, M., Benedix, G.K., Ciocco, M., Bedos, B., Guimpier, A., Dehouck, E., Loizeau, D., Bouquety, A., Zhao, J., Vialatte, A., Cormau, M., Le Conte Des Floris, E., Schmidt, F., Thollot, P., Champion, J., Martinot, M., Gargani, J., Beck, P., Boisson, J., Paulien, N., Séjourné, A., Pasquon, K., Christoff, N., Belgacem, I., Landais, F., Rousseau, B., Dupeyrat, L., Franco, M., Andrieu, F., Cecconi, B., Erard, S., Jabaud, B., Malarewicz, V., Beggiato, G., Janez, G., Elbaz, L., Ourliac, C., Catheline, M., Fries, M., Karamoko, A., Rodier, J., Sarian, R., Gillet, A., Girard, S., Pottier, M., Strauss, S., Chanon, C., Lavaud, P., Boutaric, A., Savourat, M., Garret, E., Leroy, E., Geffray, M.C., Parquet, L., Delagoutte, M.A., Gamblin, O., 2021b. Mars crater database: a participative project for the classification of the morphological characteristics of large Martian craters. Large meteorite impacts and planetary evolution VI, Vol. 550. Geological society of America 629–644.
Li, L., Yue, Z., Di, K., Peng, M., 2015. Observations of Martian layered ejecta craters and constraints on their formation mechanisms. Meteorit. Planet. Sci. 50 (3), 508–522.
Liu, Y., Wu, X., Zhao, Y.-Y.S., Pan, L., Wang, C., Liu, J., Zhao, Z., Zhou, X., Zhang, C., Wu, Y., Wan, W., Zou, Y., 2022. Zhurong reveals recent aqueous activities in Utopia Planitia, Mars. Science Advances. 8 (19), eabn8555.
Malin, M.C., Bell, J.F., Cantor, B.A., Caplinger, M.A., Calvin, W.M., Clancy, R.T., Edgett, K.S., Edwards, L., Haberle, R.M., James, P.B., Lee, S.W., Ravine, M.A., Thomas, P.C., Wolff, M.J., 2007. Context Camera Investigation on board the Mars Reconnaissance Orbiter. Journal of Geophysical Research 112 (E5), E05S04.

Marchenko, A., Basilevsky, A.T., Hoffmann, H., Hauber, E., Cook, A.C., Neukum, G., 1998. Geology of the common mouth of the Ares and Tiu Valles. Mars. Solar System Research. 32 (6), 425–452.
McCauley, J.F., 1973. Mariner 9 evidence for wind erosion in the equatorial and mid-latitude regions of Mars. J. Geophys. Res. 78 (20), 4123–4137.
Melosh, H.J., 1989. Impact Cratering: A Geologic Process. Oxford University Press, New York.
Michael, G.G., Neukum, G., 2010. Planetary surface dating from crater size–frequency distribution measurements: partial resurfacing events and statistical age uncertainty. Earth Planet. Sci. Lett. 294 (3), 223–229.
Michael, G.G., Platz, T., Kneissl, T., Schmedemann, N., 2012. Planetary surface dating from crater size–frequency distribution measurements: spatial randomness and clustering. Icarus. 218 (1), 169–177.
Michael, G.G., Kneissl, T., Neesemann, A., 2016. Planetary surface dating from crater size-frequency distribution measurements: Poisson timing analysis. Icarus. 277, 279–285.
Moore, J.M., Clow, G.D., Davis, W.L., Gulick, V.C., Janke, D.R., McKay, C.P., Stoker, C.R., Zent, A.P., 1995. The circum-Chryse region as a possible example of a hydrologic cycle on Mars: geologic observations and theoretical evaluation. Journal of Geophysical Research: Planets. 100 (E3), 5433–5447.
Moore, J.M., Asphaug, E., Belton, M.J.S., Bierhaus, B., Breneman, H.H., Brooks, S.M., Chapman, C.R., Chuang, F.C., Collins, G.C., Giese, B., Greeley, R., Head, J.W., Kadel, S., Klaasen, K.P., Klemaszewski, J.E., Magee, K.P., Moreau, J., Morrison, D., Neukum, G., Pappalardo, R.T., Phillips, C.B., Schenk, P.M., Senske, D.A., Sullivan, R. J., Turtle, E.P., Williams, K.K., 2001. Impact features on Europa: results of the Galileo Europa Mission (GEM). Icarus. 151 (1), 93–111.
Mouginis-Mark, P., 1979. Martian fluidized crater morphology: variations with crater size, latitude, altitude, and target material. J. Geophys. Res. Solid Earth 84 (B14), 8011–8022.
Mouginis-Mark, P.J., 1987. Water or ice in the Martian regolith?: clues from rampart craters seen at very high resolution. Icarus. 71 (2), 268–286.
Mutch, T.A., Binder, A.B., Huck, F.O., Levinthal, E.C., Liebes, S., Morris, E.C., Patterson, W.R., Pollack, J.B., Sagan, C., Taylor, G.R., 1976. The surface of Mars: the view from the Viking 1 Lander. Science. 193 (4255), 791–801.
Neukum, G., Hiller, K., 1981. Martian ages. J. Geophys. Res. Solid Earth 86 (B4), 3097–3121.
Neukum, G., Basilevsky, A.T., Kneissl, T., Chapman, M.G., van Gasselt, S., Michael, G., Jaumann, R., Hoffmann, H., Lanz, J.K., 2010. The geologic evolution of Mars: Episodicity of resurfacing events and ages from cratering analysis of image data and correlation with radiometric ages of Martian meteorites. Earth Planet. Sci. Lett. 294 (3), 204–222.
Pacifici, A., Komatsu, G., Pondrelli, M., 2009. Geological evolution of Ares Vallis on Mars: formation by multiple events of catastrophic flooding, glacial and periglacial processes. Icarus. 202 (1), 60–77.
Pan, L., Quantin-Nataf, C., Breton, S., Michaut, C., 2019. The impact origin and evolution of Chryse Planitia on Mars revealed by buried craters. Nat. Commun. 10 (1), 4257.
Parker, T.J., Gorsline, D.S., Saunders, R.S., Pieri, D.C., Schneeberger, D.M., 1993. Coastal geomorphology of the Martian northern plains. Journal of Geophysical Research: Planets. 98 (E6), 11061–11078.
Reiss, D., Hauber, E., Michael, G., Jaumann, R., Neukum, G., the, H.C.-I.T, 2005. Small rampart craters in an equatorial region on Mars: implications for near-surface water or ice. Geophys. Res. Lett. 32 (10), L10202.
Robbins, S.J., Hynek, B.M., 2012a. A new global database of Mars impact craters ≥ 1 km: 1. Database creation, properties, and parameters. Journal of Geophysical Research: Planets. 117 (E5), E05004.
Robbins, S.J., Hynek, B.M., 2012b. A new global database of Mars impact craters ≥ 1 km: 2. Global crater properties and regional variations of the simple-to-complex transition diameter. Journal of Geophysical Research: Planets. 117 (E6), E06001.
Robbins, S.J., Kirchoff, M.R., Hoover, R.H., 2023. Fully controlled 6 meters per pixel equatorial mosaic of Mars from Mars reconnaissance orbiter context camera images, version 1. Earth and space science 10 (3) (e2022EA002443).
Schultz, P.H., 1992. Atmospheric effects on ejecta emplacement and crater formation on Venus from Magellan. Journal of Geophysical Research: Planets. 97 (E10), 16183–16248.
Schultz, P.H., Gault, D.E., 1979. Atmospheric effects on Martian ejecta emplacement. J. Geophys. Res. Solid Earth 84 (B13), 7669–7687.
Schultz, P.H., Schultz, R.A., Rogers, J., 1982. The structure and evolution of ancient impact basins on Mars. J. Geophys. Res. Solid Earth 87 (B12), 9803–9820.
Smith, D.E., Zuber, M.T., Frey, H.V., Garvin, J.B., Head, J.W., Muhleman, D.O., Pettengill, G.H., Phillips, R.J., Solomon, S.C., Zwally, H.J., Banerdt, W.B., Duxbury, T.C., Golombek, M.P., Lemoine, F.G., Neumann, G.A., Rowlands, D.D., Aharonson, O., Ford, P.G., Ivanov, A.B., Johnson, C.L., McGovern, P.J., Abshire, J.B., Afzal, R.S., Sun, X., 2001. Mars orbiter laser altimeter: experiment summary after the first year of global mapping of Mars. Journal of Geophysical Research: Planets. 106 (E10), 23689–23722.
Smith, P.H., Tamppari, L.K., Arvidson, R.E., Bass, D., Blaney, D., Boynton, W.V., Carswell, A., Catling, D.C., Clark, B.C., Duck, T., DeJong, E., Fisher, D., Goetz, W., Gunnlaugsson, H.P., Hecht, M.H., Hipkin, V., Hoffman, J., Hviid, S.F., Keller, H.U., Kounaves, S.P., Lange, C.F., Lemmon, M.T., Madsen, M.B., Markiewicz, W.J., Marshall, J., McKay, C.P., Mellon, M.T., Ming, D.W., Morris, R.V., Pike, W.T., Renno, N., Staufer, U., Stoker, C., Taylor, P., Whiteway, J.A., Zent, A.P., 2009. H_2O at the Phoenix landing site. Science. 325 (5936), 58–61.
Squyres, S.W., Clifford, S.M., Kuz'min, R.O., Zimbelman, J.R., Costard, F.M., 1992. Ice in the Martian regolith. In: Kieffer, H.H., Jakosky, B.M., Synder, C.W., Matthews, M.S. (Eds.), Mars. The University of Arizona Press, Arizona, pp. 523–554.
Stewart, S.T., O'Keefe, J.D., Ahrens, T.J., 2001. The relationship between rampart crater morphologies and the amount of subsurface ice. In: 32nd Lunar and Planetary Science Conference. Houston, Texas, p. 2092.
Tanaka, K.L., Skinner Jr., J.A., Dohm, J.M., Irwin III, R.P., Kolb, E.J., Fortezzo, C.M., Platz, T., Michael, G.G., Hare, T.M., 2014. Geologic map of Mars, Scale 1: 20,000,000, U.S. Geological Survey Scientific Investigations Map SIM 3292. http://pubs.er.usgs.gov/publication/sim3292.
Thomson, B.J., 2018. Erosion rates on Mars: Relevance to astrobiology. In: In: 49th Lunar and Planetary Science Conference. The Woodlands, Texas, p. 1788.
Warner, N., Gupta, S., Muller, J.-P., Kim, J.-R., Lin, S.-Y., 2009. A refined chronology of catastrophic outflow events in Ares Vallis. Mars. Earth and Planetary Science Letters. 288 (1), 58–69.
Warner, N.H., Gupta, S., Calef, F., Grindrod, P., Boll, N., Goddard, K., 2015. Minimum effective area for high resolution crater counting of martian terrains. Icarus. 245, 198–240.
Weiss, D.K., Head, J.W., 2017. Evidence for stabilization of the ice-cemented cryosphere in earlier martian history: implications for the current abundance of groundwater at depth on Mars. Icarus. 288, 120–147.
Woronow, A., 1981. Preflow stresses in Martian rampart ejecta blankets: a means of estimating the water content. Icarus. 45 (2), 320–330.
Yue, Z., Di, K., Michael, G., Gou, S., Lin, Y., Liu, J., 2022. Martian surface dating model refinement based on Chang'E-5 updated lunar chronology function. Earth Planet. Sci. Lett. 595, 117765.